Beam Physics Note
TRI-BN-22-29
September 22, 2022

Beam Dynamics Study of ISAC-MEBT

Olivier Shelbaya

TRIUMF

Abstract: This report presents the ISAC-MEBT section optics and beam dynamics. Following beam development investigations which made parallel use of the TRANSOPTR model of the linac, an analysis is carried out into observed on-line behaviour of the envelopes through the medium energy section. Conclusions shed light on past issues and set the stage for a novel MEBT-DTL tuning methodology.

4004 Wesbrook Mall, Vancouver, B.C. Canada V6T 2A3 · Tel: 604 222-1047 · www.triumf.ca

The ISAC Linac & MEBT

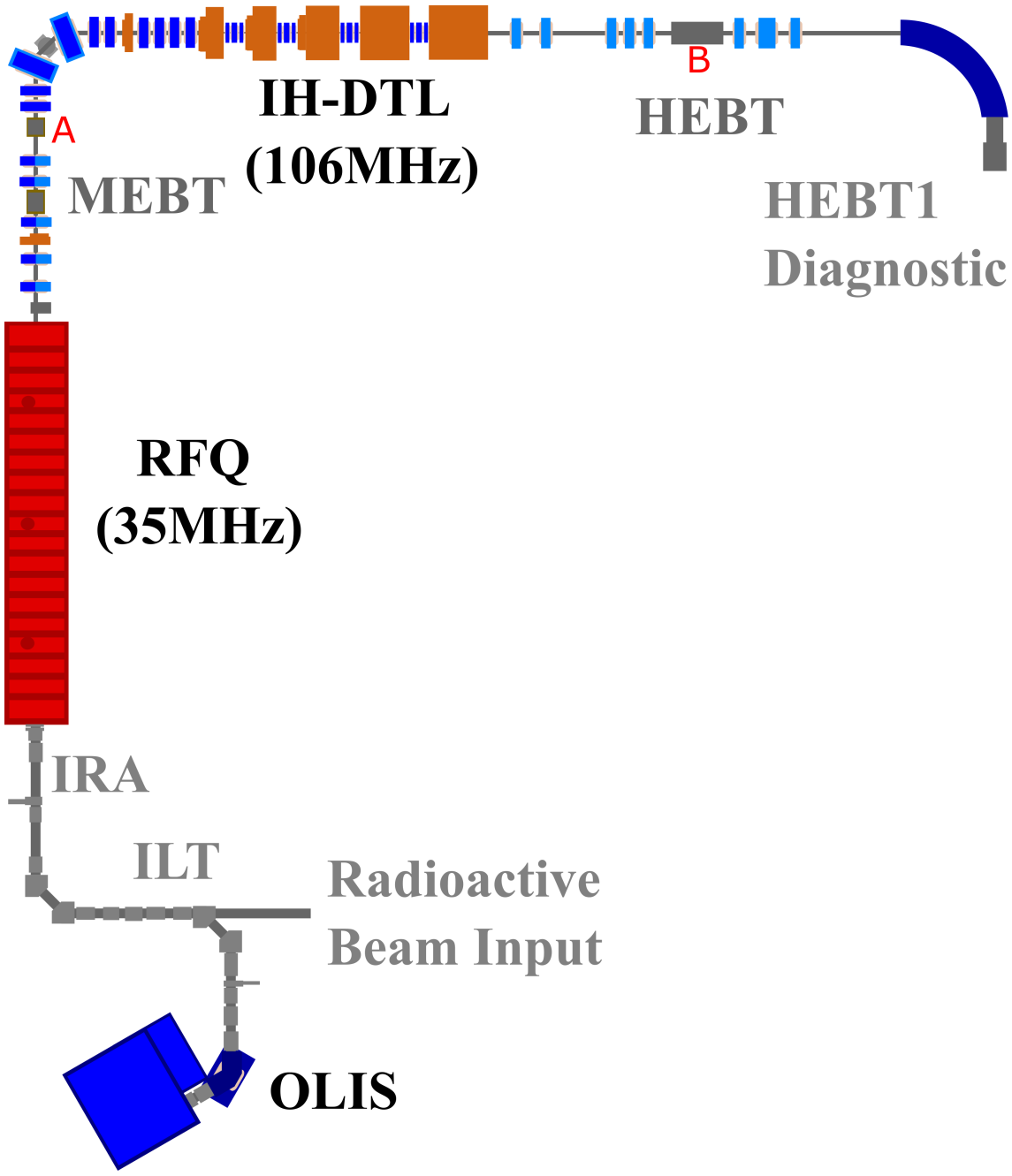

Figure 1: Schematic representation of the ISAC linear accelerator, with electrostatic beamlines before (below) the RFQ, and magnetic quadrupole optics beyond (above). The MEBT section prominently features two 45° dipoles, enabling charge state selection. Movable stripping foils at locations marked **A** and **B** allow for changes of beam charge state.

1 Beam Development Summary

This report outlines the up-to-date status of understanding of the MEBT section beam dynamics. In the 2019 report[1], an investigation of the ISAC-DTL optics was carried out, following persistent tuning difficulties by operators. The latter results in the status-quo in which the linac's optics must be manually tuned away from model values to maximize beam transmission. In the end, no issues were identified at DTL.

Difficulties persisted during beam development investigations thereafter. Quadrupole scan tomography experiments[2, 3] in the MEBT-DTL section sought to extract the beam distribution on-line, in order to compute both the MEBT and DTL quadrupole setpoints. Though the software succeeded in computing machine tunes using only the measured inputs, the on-line tunes frequently resulted in poor transmission, at or below 50% through the DTL[4].

A recurring observation in the unpowered DTL, using the linear position monitors (LPMs), was that there appeared to be a progressive mismatch in the (x, y) profiles[4]. With confidence that the DTL quadrupoles were performing nominally, scrutiny turned to the MEBT section and optics. The leading hypothesis was now that a mismatch of some kind emerged before DTL injection.

In the report [5], a drifting tune through the drift tube structure was established at high transmission (98% from MEBT to HEBT) using `TRANSOPTR` computed quadrupole optics. This tune was established by assuming the MEBT mismatch hypothesis, that is presented and reviewed in this document. But first, a useful unit of measurement for the section is introduced: The transverse beam doubling distance.

2 Beam Doubling Distance

The envelope equation for a drift can be written as:

$$\frac{\mathrm{d}\boldsymbol{\sigma}}{\mathrm{d}s} = \begin{pmatrix} \frac{2\sigma_{12}}{P_0} & \frac{\sigma_{22}}{P_0} \\ \frac{\sigma_{22}}{P_0} & 0 \end{pmatrix}. \tag{1}$$

Solve for beam matrix element 1-2:

$$\sigma_{12}(s) = \frac{\sigma_{22}}{P_0} \int \mathrm{d}s' = \frac{s\sigma_{22}}{P_0} + C_{12}. \tag{2}$$

We have pulled σ_{22} out of the integral since it is constant in a drift. Since beam starts at a waist ($\sigma_{12}(0) = 0$), we set $C_{12} = 0$. Now look at beam matrix element 1-1:

$$\sigma_{11}(s) = \frac{2}{P_0} \int \sigma_{12}(s')\mathrm{d}s' = \frac{2}{P_0} \int \left(\frac{2'\sigma_{22}}{P_0} \right) \mathrm{d}s' \tag{3}$$

$$\sigma_{11}(s) = \frac{2\sigma_{22}}{P_0^2}\left(\frac{s^2}{2} + C_{11}\right). \tag{4}$$

The constant C_{11} is found by setting $s = 0$:

$$C_{11} = \frac{P_0^2\sigma_{11}(0)}{2\sigma_{22}}. \tag{5}$$

This allows for the expression of the evolution of the squared x-envelope size ($\sigma_{11} = \langle x^2 \rangle$) along the reference trajectory s, with the waist at $s = 0$:

$$\sigma_{11}(s) = \frac{s^2\sigma_{22}}{P_0^2} + \sigma_{11}(0) \tag{6}$$

When beam doubles in size after travelling a distance s_{2x}, $\sigma_{11}(s_{2x}) = 4\sigma_{11}(0)$. Solving for s_{2x}:

$$s_{2x} = P_0\sqrt{\frac{3\sigma_{11}(0)}{\sigma_{22}}}. \tag{7}$$

For the ISAC-MEBT section, the 1 mm spot size at the chopper slit is the narrowest waist in the section and it is used to define the doubling distance. Evaluating Eq. (7) with design tune parameters taken from [6], the doubling distance is found at $s_{2x} = 17.3$ cm.

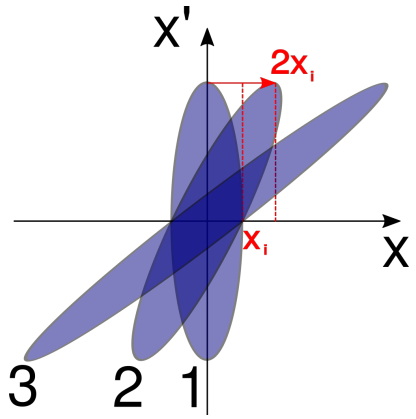

Figure 2: As an ellipse drifts from a waist (**1**), and doubles in size (**2**), the drift transformation shears the distribution. Beyond this (**3**), its eccentricity increases still. Obtained from [7].

3 The MEBT Mismatch Hypothesis

The thirteen magnetic quadrupoles in the section are identical, with effective length 18 cm[6]. The first five quadrupoles after the RFQ are tilted at 45° with respect to the conventional laboratory (x, y) frame, matching the orientation of the RFQ vanes. The design MEBT tune for $A/q \leq 6$ is shown in Figure 3. As has been pointed out by Baartman[8], a defining feature of the MEBT design tune is the straightness of the transverse beam envelopes. Envelopes with this single particle trajectory-like behaviour arise from highly eccentric phase space distributions.

Figure 4 shows the inter-quadrupole drift distances in MEBT, shown in units of this doubling distance. To understand the significance of this, the correlation coefficient r_{12} is considered, which acts as a proxy for the eccentricity of the (x, x') ellipse:

$$r_{12} = \frac{\sigma_{12}}{\sqrt{\sigma_{11}\sigma_{22}}}. \tag{8}$$

By definition, it is bound in [-1,1]. As the beam drifts from its initial waist to a doubling in size, the correlation coefficient, initially at zero reaches $r_{12} = 0.866$. Beyond this point, the eccentricity of the distribution becomes considerable, resulting in a narrow and skinny ellipse in (x, x'). Under these

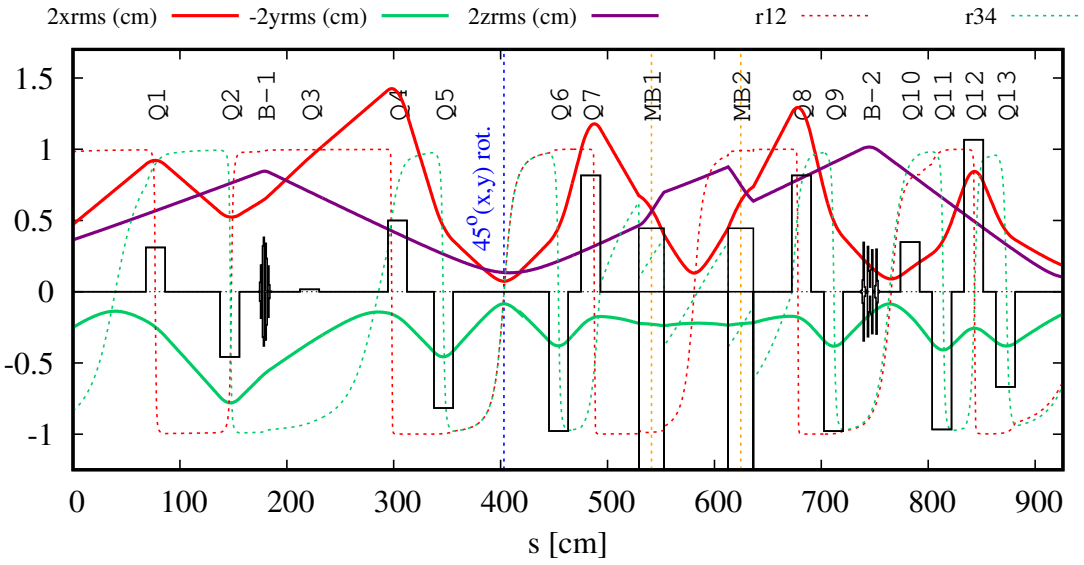

Figure 3: Design MEBT tune showcasing 2rms envelopes for (x, y, z) computed in the envelope code `TRANSOPTR`. The 45° dipoles are marked MB1 and MB2. The transverse correlation coefficients r_{12} and r_{34} are shown as dotted red and green lines, respectively. In this configuration, a longitudinal (z) focus is established at the stripping foil using the first rf buncher, with the second buncher focusing into the first DTL tank. Obtained from [7].

circumstances, the envelope is now defined by the projection of the highest momentum component of the ellipse, exhibiting a straight-line single particle trajectory-like profile. This is seen in Figure 3, which shows both r_{12} for (x, x') and r_{34} for (y, y'). Particularly striking are the considerable intervals for which $|r_{12}| \approx 1$ in MEBT. Why does this matter?

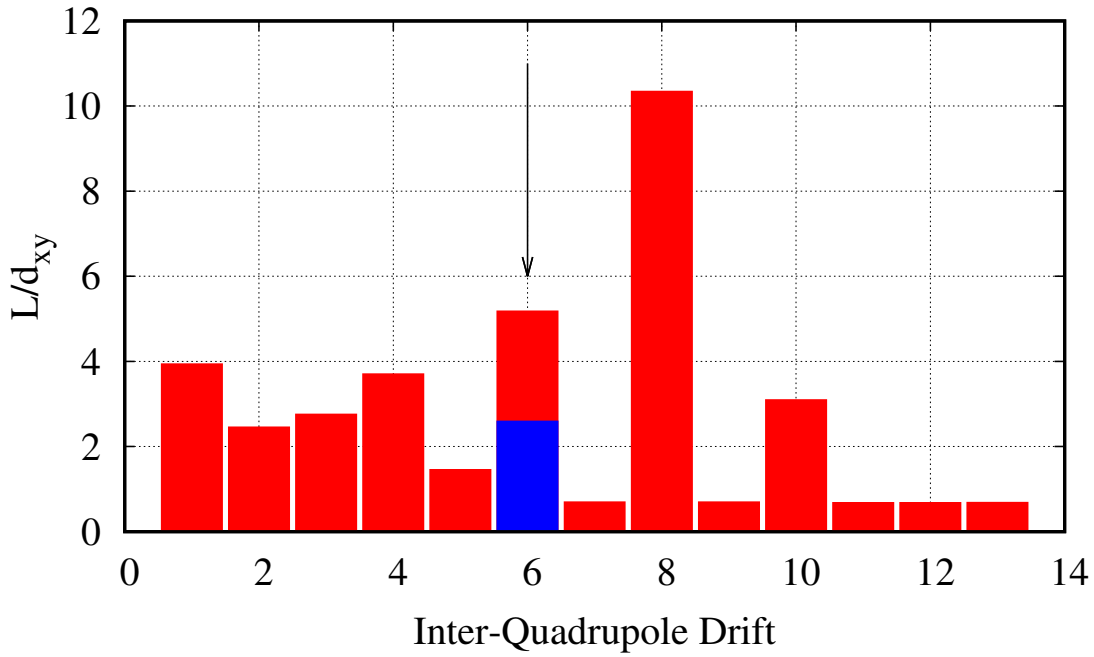

Figure 4: Beam doubling distance in the ISAC-MEBT section, measured in terms of the beam doubling distance ($s_{2x} = 17.3$ cm) from the chopper slit waist. Obtained from [7].

4 Quadrupole Transformation Errors

Start with the envelope equation:

$$\frac{\mathrm{d}\boldsymbol{\sigma}}{\mathrm{d}s} = \mathbf{F}\boldsymbol{\sigma} + \boldsymbol{\sigma}\mathbf{F}^{\mathrm{T}}, \tag{9}$$

concentrating on only (x, x'), assuming an uncoupled beam. We want to find the s-derivative of the beam matrix through a magnetic quadrupole with pole-tip field B and gradient B', with strength parameter $k = B'/(B\rho)$. The top-leftmost 2x2 terms in the F-matrix for a magnetic quadrupole are:

$$\mathbf{F} = \begin{pmatrix} 0 & \frac{1}{P_0} \\ \frac{-Eqk}{c^2 P_0} & 0 \end{pmatrix}. \tag{10}$$

Evaluating (9) using (10) and a general 2x2 $\boldsymbol{\sigma}$-matrix, we can write:

$$\frac{\mathrm{d}\boldsymbol{\sigma}}{\mathrm{d}s} = \begin{pmatrix} \frac{2\sigma_{12}}{P_0} & \frac{c^2\sigma_{22} - E\sigma_{11}qk}{c^2 P_0} \\ \frac{c^2\sigma_{22} - E\sigma_{11}qk}{c^2 P_0} & \frac{-2E\sigma_{12}qk}{c^2 P_0} \end{pmatrix}. \tag{11}$$

Let us assume that a small and a priori unknown magnetic field error causes a strength error: $k \longrightarrow k + \Delta k$. Performing this substitution in (11), the (x, x') envelope inside the quadrupole will evolve as:

$$\left.\frac{\mathrm{d}\boldsymbol{\sigma}}{\mathrm{d}s}\right|_{k \longrightarrow k+\Delta k} = \frac{\mathrm{d}\boldsymbol{\sigma}}{\mathrm{d}s} + \mathbf{R}, \tag{12}$$

$$\mathbf{R} = \begin{pmatrix} 0 & \frac{-E\sigma_{11}q\Delta k}{c^2 P_0} \\ \frac{-E\sigma_{11}q\Delta k}{c^2 P_0} & -2r_{12}\sqrt{\sigma_{11}\sigma_{22}}\frac{Eq\Delta k}{c^2 P_0} \end{pmatrix}. \tag{13}$$

Where the $\boldsymbol{\sigma}$-matrix transforms through the quadrupole with an error matrix $\mathbf{R}$, proportional to Δk. By inspection, the error matrix will not directly affect the size of the beam, with $\mathbf{R}_{11} = 0$. Instead, the transformation error upon the beam matrix will cause an effect in both the transverse momentum and r_{12}. Since $\mathbf{R}_{22} \propto r_{12}$, the momentum error will be larger for more highly eccentric distributions. The error term $\mathbf{R}_{12} = \mathbf{R}_{21}$ is beamsize dependent. The overall mismatch caused by $\mathbf{R}$ can thus be expected to become apparent further downstream.

Figure 5 shows (x, r_{12}) starting from the waist at the chopper slit. Beam doubling distance is shown as a vertical dotted line. Upon entry into Q6, the x-envelope has roughly tripled in size while the correlation coefficient is above 0.9. The quadrupole then defocuses beam, further increasing the eccentricity and sending r_{12} near unity by Q7's entrance. The distribution upon entrance into Q7 is shown to the left of Fig. 6. Per (13), since $r_{12} \approx 1$ and since the extent of σ_{22} is large when compared to the vertical envelopes, Q7 produces a transformation which is sensitive to any quadrupole tip-field error, shown to the right of the same figure.

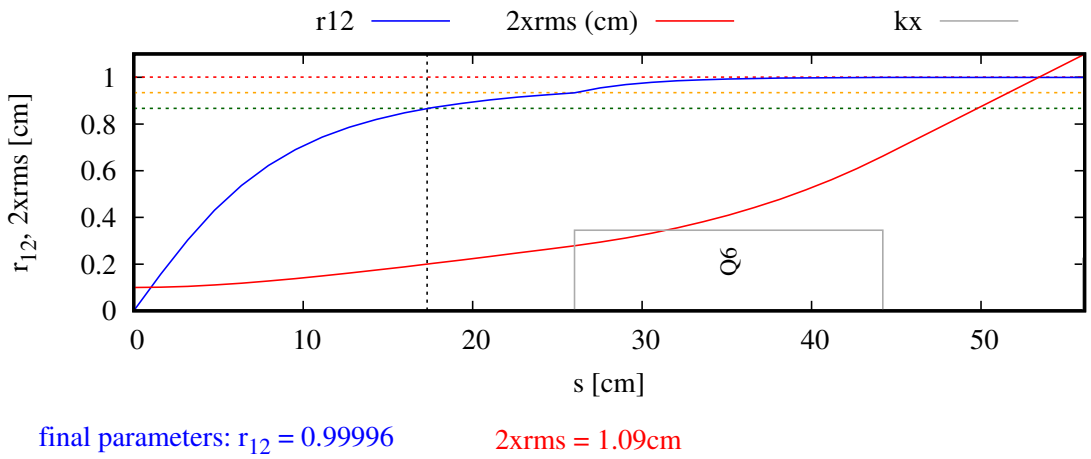

Figure 5: 2rms (x, x') envelopes and r_{12}, starting at chopper-slit and ending at start of Q7. Dashed lines show $r_{12} = 0.866$ (green), $r_{12} = 0.933$ (yellow) and $r_{12} = 0.999$ (red). Beam parameters at Q7 are shown at the bottom.

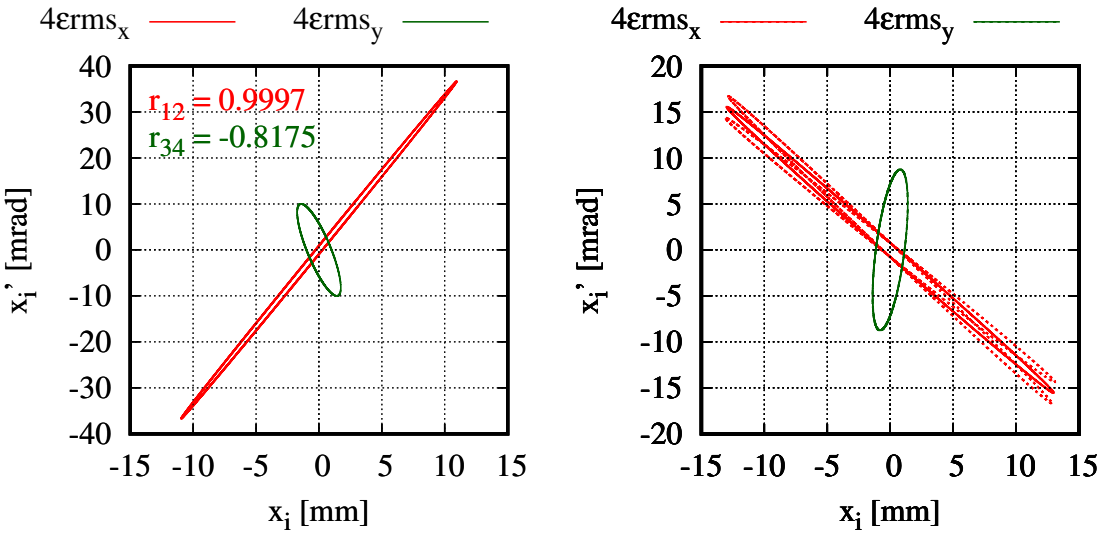

Figure 6: 4ϵrms (x, y) beam containment ellipses computed in TRANSOPTR at the entrance of MEBT:Q7 (**Left**). A ± 5 mT tip-field error has been applied, causing the transformation errors shown as the dotted red ellipses (**Right**). Correlation coefficients r_{12} and r_{34} shown. Obtained from [7].

5 Chromaticity

In the MEBT corner, the beam matrix sees the emergence of nonzero terms between dimensions 1,2 and 5,6, as shown in Figure 7. Since the longitudinal distribution through the corner is defined by the bunch rotator cavity, variation of its parameters or even those of the ISAC-RFQ may also affect the envelopes through the 90° bend.

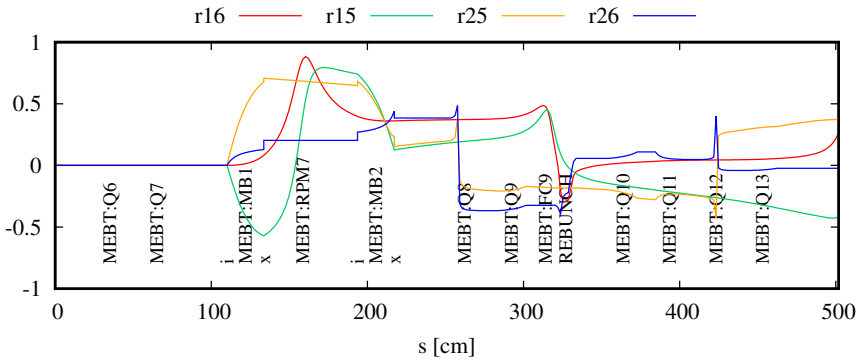

Figure 7: Beam matrix correlation coefficients between canonical coordinates in `TRANSOPTR`. An A/q = 30/5 beam has been used at E/A = 0.153 MeV/u. Obtained from [7].

To understand the behavior of the σ-matrix between Q7 and Q8, it is important to consider the effects of chromaticity that this causes. The section is singly achromatic, not doubly achromatic [9], owing to the absence of inter-dipole quadrupoles in the design. This means that the dispersion[10] function will be zero at one location downstream of the bend, but with nonzero derivative. Dispersion returns to nonzero values away from this location. We therefore expect the injected distribution in the DTL to possess nonzero couplings amongst the (x, x') and (z, z') planes.

6 Longitudinal Envelopes

Two rf cavities define the MEBT section, with more details in [6]. The bunch rotator is used to establish a z-waist at the stripping foil location, while the rebuncher is used to establish another z-waist in the first IH tank of the DTL. The (z, z') envelopes in MEBT are shown in Figure 8, together with r_{56}. Beam exits the RFQ diverging in (z, z'), evidenced by the initial value of $r_{56} > 0.9$ in the section. Thus, establishment of a time-focus at the stripping foil causes an increase in the longitudinal momentum spread of the beam. During transit through the corner, nonzero correlations emerge in the beam matrix as shown in Figure 7. Since chromatic couplings depend on the magnitude of coordinate-6 (z'), the time-focus will accentuate the downstream effects of beam chromaticity post-MEBT corner.

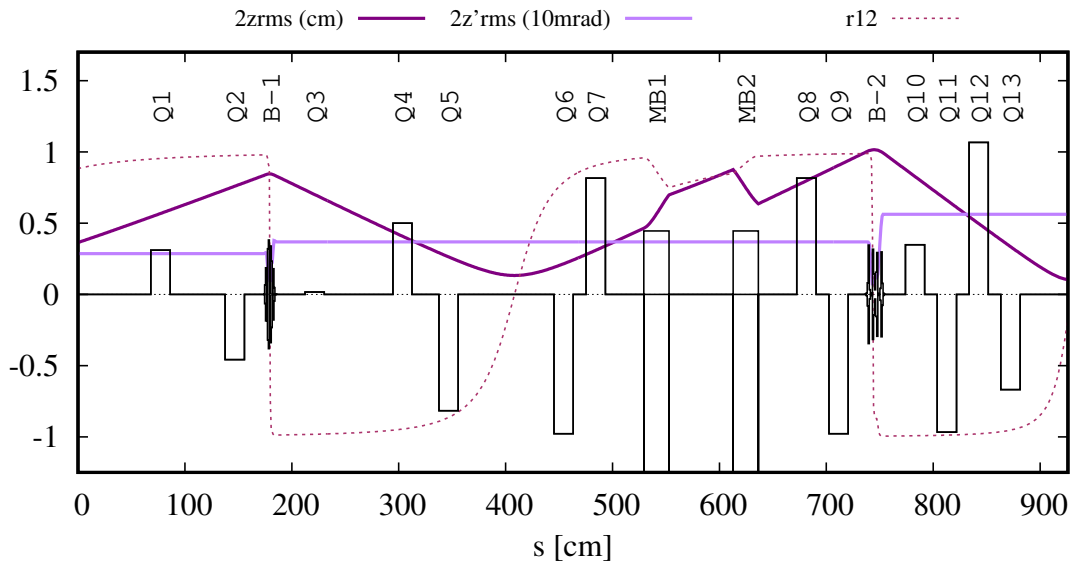

Figure 8: TRANSOPTR simulation of the design longitudinal MEBT tune, with a time-focus at the stripping foil location established by the first MEBT rf cavity. The re-buncher in turn establishes a time-focus at the first IH structure in the DTL. This causes increases to the longitudinal momentum envelope, causing it to double by the section's exit, where correlations between (x, x') and (z, z') are nonzero (Fig. 7).

Use of the MEBT rebuncher to capture z-diverging beam exiting the corner and establish another time-focus into the first IH structure causes another increase in z', which leaves the section roughly double its initial value out of the RFQ.

7 Monte-Carlo DTL Mismatch Simulations

The effects described thus far, both transverse and longitudinal, act together to produce a mismatch condition at DTL injection. Simulations of the section using TRANSOPTR can illustrate this. Looking back to the inter-quadrupole drift distances (Figure 4) in terms of the chopper-slit waist doubling distance, the 8th drift between MEBT:Q7 and Q8 is the largest in the section: These quadrupoles define the MEBT corner. Between them are the two dipole magnets MB1 and MB2.

The effect of small quadrupole field errors, for example due to an unknown hysteresis error[11], are now considered. A TRANSOPTR simulation has been defined, starting at the chopper-slit and terminating at the entrance of the first DTL IH tank. A monte-carlo simulation has been performed, consisting of 250 iterations during which gaussian distributed pseudo-random $\pm 5\,mT$ errors are applied to each quadrupole. Each individual quadrupole receives a different error at each iteration.

The resulting envelopes are processed to obtain both the centroid at each location s along the reference trajectory, in addition to the variance in envelope size. Both are shown to the left of Figure 9. In the dispersive plane (x), a considerable mismatch emerges after transit through Q7, at injection into the DTL. Figure 9 shows the Bovet mismatch parameter $\mathcal{D}$ [12] for both (x, y) at the entrance of Tank-1. Though a slight vertical mismatch can emerge, it is clear that the issue is principally in the horizontal plane.

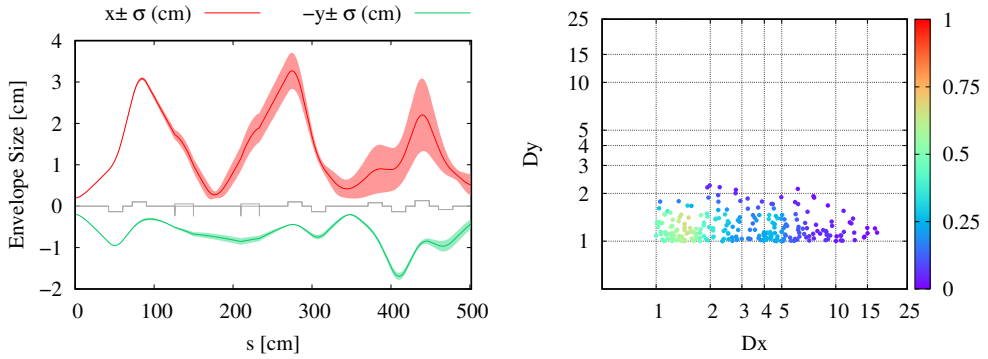

Figure 9: **Left:** Envelope mean and variance for randomly computed ± 5 mT quadrupole tip-field errors, over 250 iterations. **Right:** The Bovet mismatch parameters $\mathcal{D}$ have been computed at each iteration for (x, y). Local density of points shown with colorscale. Obtained from [7].

This mismatch causes envelope size variations through DTL. Figure 10 shows the simulation propagated through the unpowered linac. Subroutine `slit`[13] has been used to simulate DTL apertures. The MEBT mismatch causes mainly horizontal collisional losses. This can also cause a stronger sensitivity on beam alignment through the accelerator.

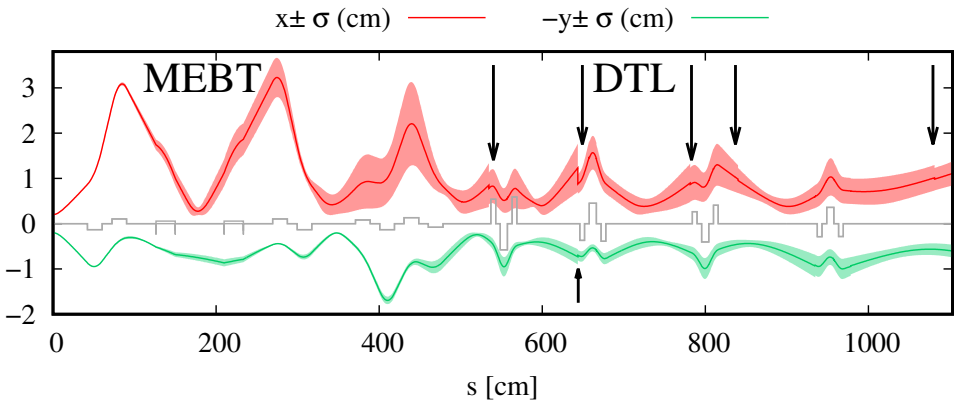

Figure 10: Envelope mean and variance for randomly computed ± 5 mT quadrupole tip-field errors, over 250 iterations. Beam starts at the MEBT chopper slit and ends at the exit of the ISAC-DTL. The mismatch leads to aperture collisions (arrows) mainly in x, the dispersive plane, causing transmission loss. Obtained from [7].

8 Conclusions

- Beam development has identified that transverse tuning difficulties at DTL appear to arise from a mismatch in the MEBT section.
- Analysis of the MEBT tune: Error arises due to highly eccentric distributions, rendering the optics sensitive to small gradient errors.
- A new MEBT tuning method has been shown: Using `TRANSOPTR` computed DTL quadrupoles, the MEBT optics are detuned from their `tuneX` values, producing high transmission. This was tested without a stripping foil[5].
- Chromatic couplings emerge in the MEBT corner, as there are no inter-dipole quadrupoles. Additionally, time-focussing the beam at the stripping foil with the rotator cavity increases energy spread into the corner.
- This potentially couples diurnal rf phase drifts[14] to the size in the DTL (Fig. 10).
- The above potentially explains diurnal transmission variations[15], shown in Figure 11.
- An identified overfocus of the bunch rotator for $A/q \leq 4.5$[16] potentially made these effects of greater magnitude, by way of broadening the longitudinal energy spread into the corner.
- This knowledge should be used to elaborate a new tuning method for the ISAC-MEBT section, working together with operators.

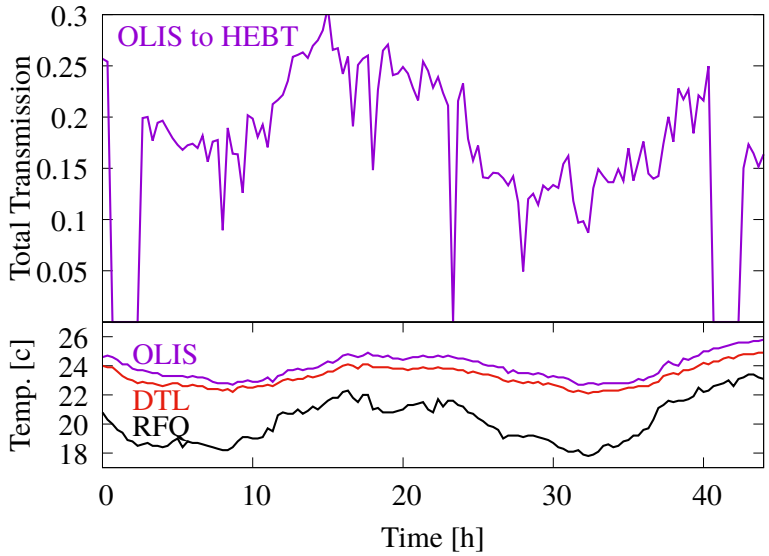

Figure 11: Observed diurnal-like temperature-transmission correlations observed at ISAC over a 48 h period, obtained from [15].

References

[1] Olivier Shelbaya and Richard Baartman. Langevin-Like DTL Triplet BI Fits and Analysis of Transverse DTL Tuning Difficulties. Technical Report TRI-BN-19-18, TRIUMF, 2019.

[2] Jedri de Luna. Phase Space Tomography at TRIUMF. Technical Report TRI-BN-19-23, TRIUMF, 2019.

[3] Olivier Shelbaya. Maximum Entropy Tomography at the ISAC-RFQ. Technical Report TRI-BN-20-12, TRIUMF, 2020.

[4] Olivier Shelbaya. Status of Model Coupled Accelerator Tuning at ISAC-I. Technical Report TRI-BN-21-07, TRIUMF, 2021.

[5] Olivier Shelbaya. Model Coupled DTL Drifting Tune On-Line . Technical Report TRI-BN-22-13, TRIUMF, 2022.

[6] Olivier Shelbaya. TRANSOPTR Implementation of the MEBT Beamline. Technical Report TRI-BN-19-02, TRIUMF, 2019.

[7] O. Shelbaya. *Model Coupled Accelerator Tuning*. PhD thesis, University of Victoria, Department of Physics and Astronomy, 2022. (Unpublished).

[8] R. Baartman. personal communication.

[9] RE Laxdal and M Marchetto. *The ISAC post-accelerator. Hyperfine Interactions*, 225(1-3):79–97, 2014.

[10] A Verdier. Chromaticity (particle accelerators). Technical Report 10.5170/CERN-1995-006.77, CERN, 1995.

[11] J. Nasser, R.A. Baartman, O.K. Kester, S. Kiy, T. Planche, S.D. Rädel, and O. Shelbaya. Algorithm to Mitigate Magnetic Hysteresis in Magnets with Unipolar Power Supplies. In *Proc. IPAC'22*, number 13 in International Particle Accelerator Conference, pages 156–159. JACoW Publishing, Geneva, Switzerland, 07 2022.

[12] Claude Bovet, Robert Gouiran, Igor Gumowski, and Karl Helmut Reich. A selection of formulae and data useful for the design of A.G. synchrotrons; rev. version. Technical Report CERN-MPS-SI-Int-DL-70-4, CERN, Geneva, 1970.

[13] Richard Baartman. SLIT routine for TRANSOPTR. Technical Report TRI-BN-19-21, TRIUMF, 2019.

[14] Spencer Kiy. LLRF Phase Shifter Calibrations, October 2020 . Technical Report TRI-BN-20-19, TRIUMF, 2020.

[15] Olivier Shelbaya and Oliver Kester. Toward an End-to-End Model for ISAC-I Accelerators. *J. Phys. Conf. Ser.*, 1067(6):062028, 2018.

[16] Olivier Shelbaya. Overfocusing of the MEBT Bunch Rotator . Technical Report TRI-BN-21-18, TRIUMF, 2021.